A nonlinear approach to the wind strength of Gothic Cathedrals: the case of Notre Dame of Paris

Filippo Masi, Ioannis Stefanou, P Vannucci

A nonlinear approach to the wind strength of Gothic Cathedrals: the case of Notre Dame of Paris

F. Masi[1,2], I. Stefanou[2], and P. Vannucci*[3]

[1]Department of Industrial Engineering, University of Florence (I).

[2]Laboratoire Navier - UMR8205, CNRS, ENPC & IFSTTAR.
Université Paris-Est, Marne La Vallée (F)

[3]LMV, Laboratoire de Mathématiques de Versailles - UMR8100 CNRS & UVSQ.
University Paris-Saclay, Versailles (F)

February 6, 2017

Abstract

The problem of assessing the strength to wind actions of Gothic Cathedrals is addressed in this paper. A nonlinear approach, based upon a large-strain, large displacements formulation and using a nonlinear constitutive law modeling the no-tension behavior of the material as a damage law is proposed. The method is applied to the study of the Cathedral Notre Dame of Paris.

Key words: Wind actions, Gothic Cathedrals, nonlinear FEM, Notre Dame of Paris

1 Introduction

Gothic Cathedrals are one of the most important cultural heritages of Europe. They characterize the panorama of several European towns and prove the skill and boldness of the architects of the Middle Ages. Though unaware of the laws of physics, they dared, simply using their experience and flair, to conceive audacious buildings that defy the laws of mechanics since eight centuries. Designing such structures with the same materials, just stone and mortar, should be also today a real challenge and maybe a nightmare for any modern engineer, supplied by the most up to date computing means and methods.

As very imposing and articulated stone structures, Gothic Cathedrals are the object of different studies, aiming at understanding, on one hand, the way these structures have been conceived and, on the other hand, how much safe they are, namely with respect to the self weight loads and the wind thrust.

*Corresponding author: Paolo Vannucci. LMV, 45 Avenue des Etats-Unis. 78035 Versailles, France
E-mail: paolo.vannucci@uvsq.fr

Rather surprisingly, there are few studies on this last problem; without going back to old treatises, like [Ungewitter, 1890], treating classically the problem of lateral forces using the method of the thrust line, a fundamental work has been that of R. Mark. In his book *Experiments in Gothic Structure*, he tackles the analysis of the lateral wind forces on a Gothic Cathedral using the experimental technique of photoelasticity, [Mark, 1982].

It is interesting to notice that R. Mark investigated, with this technique, the response of Notre Dame of Paris as built before the structural modifications made after 1225. The motivation of his study is in his own words:

> *This relatively lightly constructed central vessel of the Cathedral Notre Dame is thirty-three meters from floor to vault keystone, a full eight meters taller than its highest Gothic predecessors, the Cathedrals of Laon and Sens, and the largest single-incremental height increase for a new church over an earlier building in the entire era. Since wind speeds are greater at higher elevations, and wind pressure is proportional to the square of the speed, earlier experience with lower-profiled, more heavily massed churches could not have fully prepared the builders to cope with the new environment. Because of massive reconstructions made to Notre Dame after 1225, just how the design problem was solved in the original Gothic construction remained unclear* [Mark, 1984].

His objective was hence to understand if the modifications made by the architects of the XIII-th century were motivated by some structural reasons, and not exclusively by architectural and stylistic ones. In particular, R. Mark has shown that the original structure, with a different arrangement of the flying buttresses, had some structural problems. Namely, he showed that under the wind action of heavy storms, tensile stresses exceeding three to five times the tensile admissible stresses for the mortars of the Middle Ages arose in some part of the structure, so certainly producing evident cracks. This can explain, in the opinion of R. Mark, why the structure was modified after 1225. The present structure of the Cathedral is shown in Fig. 2, while the original one is presented in Fig. 3; the structural differences, mainly concerning the flying buttresses, are evident.

R. Mark made experiences with photoelasticity also on other Cathedrals, namely Amiens and Beauvais, [Mark, 1982]. However, it is worth recalling that the underlying assumption of photoelasticity is the linearly elastic overall behavior of the structure, assumption that can be considered as correct only for analyses that are restrained to situations where there are not significative cracks arising in the structure. This exactly happens when the structure approaches its ultimate state under extreme winds. So, such an approach cannot be used to determine the ultimate wind strength of a Cathedral.

A more recent work is that of M. Como and his team, [Como, 2013], [Coccia et al., 2015]. In a research concerning the Amiens Cathedral, the study of the lateral wind strength is done using the limit analysis method, i.e. calculating the ultimate load multiplier λ_{cr} of the wind pressures over the lateral parts of the Cathedral. For $\lambda = \lambda_{cr}$, the structure is transformed into a mechanism by the formation of a sufficient number of plastic hinges, i.e. rotation points formed by the cracking of the stone masonry under the action of tensile stresses. The theoretical framework is that defined by Heyman, [Heyman, 1995], i.e. the masonry has no tensile strength at all, the compressive strength can be considered as infinite and no sliding failures occur in the structure. Actually, in [Coccia et al., 2015] also local sliding mechanisms are anyway considered.

The study is conducted on a planar scheme, obtained considering a transversal portion of the Cathedral between two successive pillars of the main aisle. The two analyses make use of slightly different hypotheses for the calculation of the wind pressure, which finally results in two different values of the ultimate wind speed at 10 m above the ground, which passes from 146 km/h in the first study to 109 km/h in the second one.

Such wind speed values have been exceeded in France rather frequently, also during recent extreme events: a velocity of 220 km/h has been recorded at Cap Finistère, in Bretagne, on October 15, 1987. During the storms of December 26 and 28, 1999, a wind speed of 169 km/h has been measured at Parc Montsouris, inside the city of Paris, while during the storm Xynthia, February 28, 2010, the wind has reached the speed of 136 km/h at Metz, well far from the coasts. Very recently, on January 12, 2017, the storm Egon has produced wind gusts at 146 km/h at Dieppe and has destroyed the rose of the Cathedral of Soissons.

These few data show that extreme wind storms, potentially able to produce important structural damages and possibly the ruin of tall buildings, are rather frequent. Such events are hence to be taken into consideration carefully. This is even more needed today, for climate deregulation produced by global warming has rendered meteorological phenomena statistically non stationary. The result is that the forecast of extreme events, and in particular the evaluation of the return period of such an occurrence, is today really uncertain. Nevertheless, the recent historic records of wind storms clearly show that the structural analyses of important historical buildings like Gothic Cathedrals, more sensitive to such events due to their dimensions and type of structure, are today necessary.

To this purpose, we have studied the response to a lateral wind of the Cathedral Notre Dame of Paris, with the intention of determining its ultimate strength: our goal was to bound the critical wind, the one able to produce the global failure of the structure and, possibly, to give a reliable assessment of its value. We have followed a different approach with respect to the studies cited above. In particular, we performed an incremental analysis in order to determine the response of the structure, in terms of horizontal displacements, to different wind velocities. When the equilibrium of the structure is no more reached, the failure occurs.

This choice has been inspired by three considerations: on one hand, to perform a limit analysis on a five-aisles Cathedral with galleries is much more cumbersome than the same analysis on a Cathedral of the High Gothic period, like that of Amiens, with only three aisles and no galleries, [Jantzen, 1957], [Simson, 1962], [Frankl, 1963], [Wilson, 1990], because to determine all the possible failure mechanisms, global and local, is very delicate.

On the other hand, the incremental approach that we have used allows to find, for each wind speed considered, the equilibrium configuration. It lets appear the progressive damage of the structure and eventually the failure wind and mechanism. It is interesting to notice that we find a precise failure mechanism, well identified on a 3D structure.

Finally, the deformation of the structure is determined for each incremental value of the wind action, so letting appear the time response of the Cathedral to wind. However, because we do a quasi-static analysis, where all dynamical effects are neglected, the time is a synthetic one, a purely numerical quantity that cannot be transformed into a physical

time. Nonetheless, by this procedure we can draw curves simulating the time response of the Cathedral.

All the simulations have been done on a finite element model of a *unit* element of the main aisle, specified below. The simulations are non-linear, because of the constitutive equation, a softening law representing the tensile damage of the material, used to model the no-tension behavior of stone masonry (material nonlinearity), and because we have done them considering large deformations and displacements (geometric nonlinearity), that occur when the structure is close to its ultimate state.

This paper is organized as follows: in Sect. 2 we introduce the structure of the Cathedral Notre Dame of Paris and its finite element model. In Sect. 3 we detail the constitutive law used to model the material and in Sect. 4 the representation of the wind loads. The details about the numerical procedure and simulations are given in Sects. 5 and 6, while some final considerations are presented in Sect. 7.

2 The structural model

The Cathedral Notre Dame of Paris, one of the principal examples of the Early Gothic period, has been built from 1163 and during about one century. Its overall dimensions are: length 130 m, width 48 m, height of the vaults 32.5 m, total height, comprehending the timber roof, 45 m. The high vault of the main aisle is built with a sexpartite scheme, i.e. each vault is composed by six webs. The scheme of the structure is shown in Figs. 1 and 2. The Cathedral has five aisles plus the lateral chapels and wide galleries that run all along the principal aisle and round the choir.

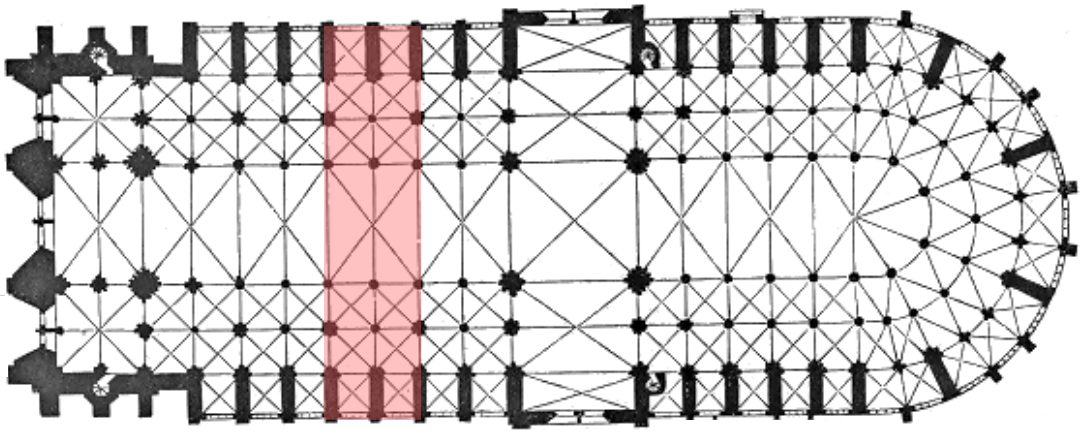

Figure 1: Plan of Notre Dame of Paris

The geometry of Notre Dame of Paris is hence particularly complex and articulated, much more than other Cathedrals of the High Gothic period, like Chartres, Reims or Amiens, where galleries are not present and the aisles are only three. Also the dimensions are different: though when it was built it was the highest Cathedral, for the race to height typical of Gothic architecture it soon was exceeded in height by other Cathedrals. A sketch of the historical evolution of the height of French Gothic Cathedrals is given in Fig. 3.

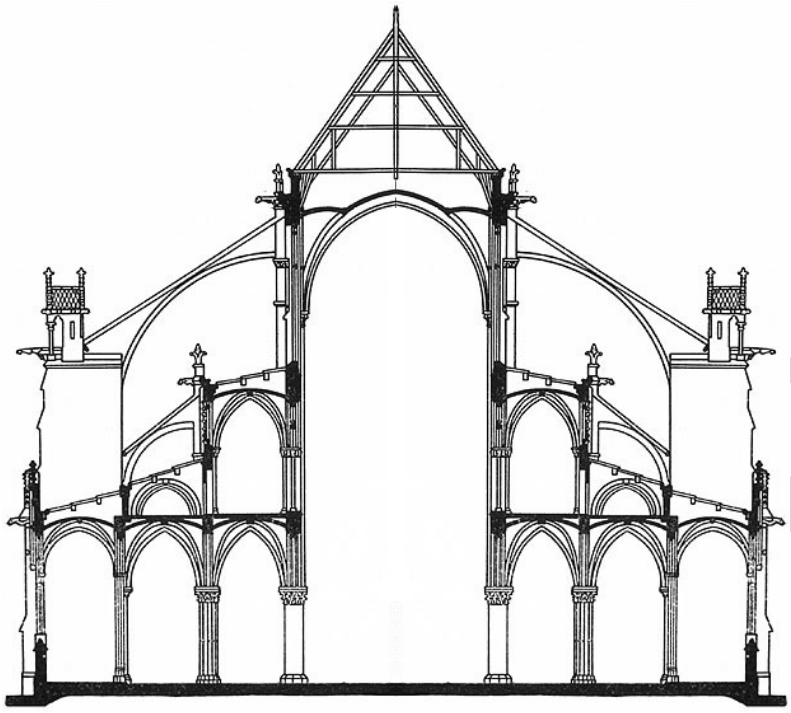

Figure 2: Transversal section of Notre Dame of Paris (as it is at present, after the modifications started in 1225 and the restoration of Viollet-le-Duc, XIXth century).

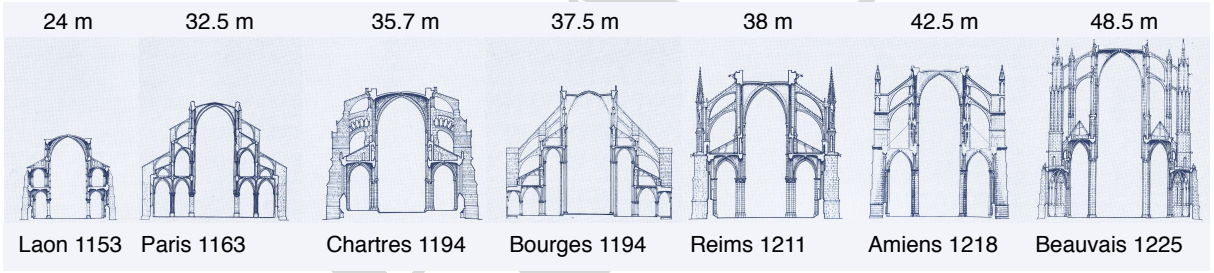

Figure 3: Historical evolution of the Gothic Cathedrals height (from [Mark, 1984]).

This point is important for two reasons: first, the transversal section is very stiff and strong and, second, its height is less than that of other major Cathedrals, like Amiens or Beauvais. For these reasons, the Cathedral of Paris is probably less sensitive to wind actions than other Gothic Cathedrals. Nevertheless, it is interesting to analyze its strength to lateral wind actions and compare it with the results found by Como and co-workers for the Cathedral of Amiens.

For this study, we have considered a structural *unit*, i.e. the part of the Cathedral shadowed in Fig. 1. It comprehends a complete sexpartite vault, 12 m in length, and the entire width of the Cathedral. A detailed numerical model has hence been done, represented in Figs. 4 to 6, based upon a survey of the Cathedral and the laserscan done by A. Tallon, of Vassar College, available on the web, [Tallon, 2010].

Due to the complexity of the Gothic architecture, some geometrical simplifications, not affecting the overall structural response of the Cathedral, have been done. In particular, all the parts that are merely decorative are not taken into account−i.e. crockets, windows,

traceries and pinnacles. The ribbed vaults are modeled carefully, together with the pointed arches and the flying buttresses, since the stability and integrity of the whole building depend on them. Also, the filling in the springing zone of the vaults have been modeled until an angle of 30° on the horizontal, see Fig. 6.

In order to avoid a meaningless growth of the finite element model, and as a consequence of the computational effort, the roof of the building has been modeled just to take on the wind actions. So, it is modeled by two rigid inclined plates whose top is 10 m above the guttering walls, like in the Cathedral. The roof, made of lead and wood, applies an estimated linear load of 2×10^4 N/m on the top of each one of the guttering walls. All the simulations have been done using the commercial code ABAQUS.

Figure 4: The numerical model of Notre Dame of Paris: overall view.

Taking advantage of its symmetry, calculations have been made just using one half of the structural *unit*, i.e. a portion of the Cathedral of 6 m in length, indicated in blue in Fig. 7. This allows to reduce the degrees of freedom and hence the run duration of the simulations.

The finite element discretization used in the simulations consists of tetrahedral elements, supported by both the standard and explicit solvers of ABAQUS, with an average element size of 0.2 m, in which *ad-hoc* refinements are pursued in some parts, due to the complexity of the geometry. The fineness of the mesh has been chosen after a convergence analysis, presented below, performed in order to obtain a reliable degree of accuracy with an acceptable length of the computing time. This gives, in the end, a finite element model with 1.83 millions of elements for a total size of the model of 1.25 millions degrees of freedom. Details of the final mesh, used in the simulations, are shown in Fig. 8.

As the simulations are planned to be done by a two-step approach, see Sect. 5, we have validated the model using first a standard (implicit) scheme and then an explicit one. The

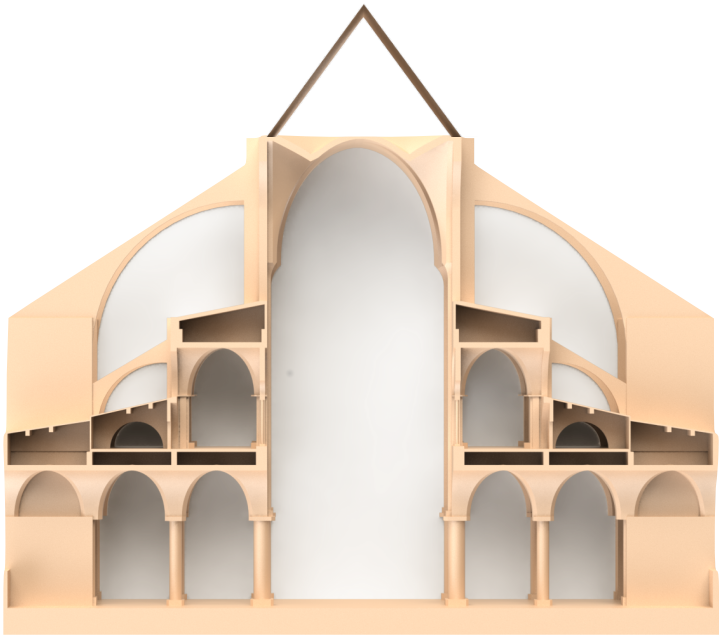

Figure 5: The numerical model of Notre Dame of Paris: transversal section.

response in both the cases has been evaluated on the eigenfrequencies of the first twenty vibration modes of the structure and on the vertical displacement of the boss of the high vault, the point indicated as V in Fig. 7, under the action of gravity.

The standard analysis is divided into two parts, namely a modal analysis and a static one with the gravity load. Both of these analyses have been made for eleven different meshes m, whose characteristics are given in Tab. 1.

Table 1: Characteristics of the studied meshes m.

m	Average element size $[m]$	Number of elements	Number of nodes
1	0.10	10616614	2101473
2	0.15	3432785	724257
3	0.20	1830092	406342
4	0.30	524967	130153
5	0.40	268222	70918
6	0.50	162751	45476
7	0.60	112388	32781
8	0.80	71952	21714
9	1.00	54474	16684
10	1.50	33396	10607
11	2.00	25827	8336

The first twenty eigenfrequencies f_m^j, $j = 1, 2, \ldots, 20$, and the vertical displacement of the point V of the sexpartite vault, u_m, are calculated for each mesh m. The convergence of the mesh has been evaluated calculating $\forall m$ the errors Δf_m^j of the frequencies f_m^j and Δu_m of the displacements u_m, relatively to the same quantities calculated for the reference

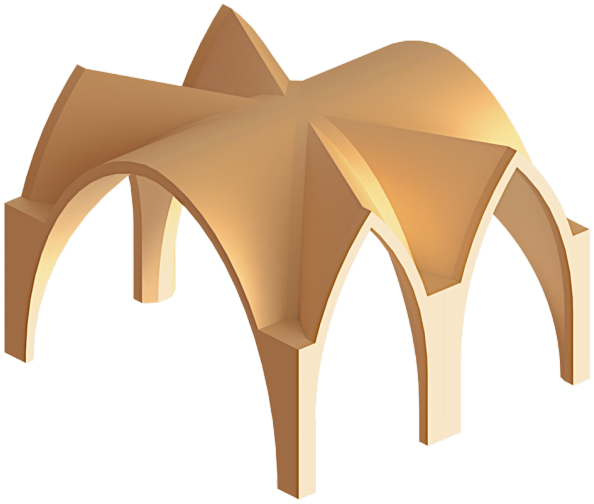

Figure 6: The numerical model of Notre Dame of Paris: the sexpartite vault.

mesh, the finest one, $m = 1$, having an average element size of 0.10 m:

$$\Delta f_m^j = \left| \frac{f_m^j - f_1^j}{f_1^j} \right|, \quad j = 1, 2, \ldots, 20, \qquad \Delta u_m = \left| \frac{u_m - u_1}{u_1} \right|. \tag{1}$$

In Fig. 9 we show the relative errors for the frequencies of the 1^{st}, 10^{th} and 20^{th} vibration modes of the structure along with that of the displacement of point V, in function of the number of elements of each mesh m.

A similar procedure was followed for investigating the mesh convergence for the explicit analysis. A mass proportional damping is applied in order to dissipate any oscillations due to the dynamic character of the analysis and to reach equilibrium faster. The convergence of the explicit analysis has been studied on the meshes $m = 2, 3, 11$, having an average element size of 0.15, 0.20 and 2.00 m respectively. The results are given in Tab. 2, where they are compared with the corresponding values of the standard (implicit) analysis. Also for the explicit analyses, the values of Δu_m have been normalized using eq. (1), i.e. using the value of $u_{m=1}$ calculated with the implicit scheme.

Table 2: Comparison of the relative errors for the vertical displacement of point V, calculated for three meshes with the implicit and explicit procedures.

m	Number of elements	Δu_m implicit [%]	Δu_m explicit [%]	Difference implicit-explicit [%]
2	3432785	0.64	0.28	0.36
3	1830092	0.84	0.36	0.48
11	25827	22.40	21.81	0.59

There are some very small differences between the explicit and the implicit analyses, to be imputed to some differences in the finite element formulation between the *ABAQUS Explicit* and *ABAQUS Standard* (implicit) solvers. Such differences are meaningless for the purpose of this study.

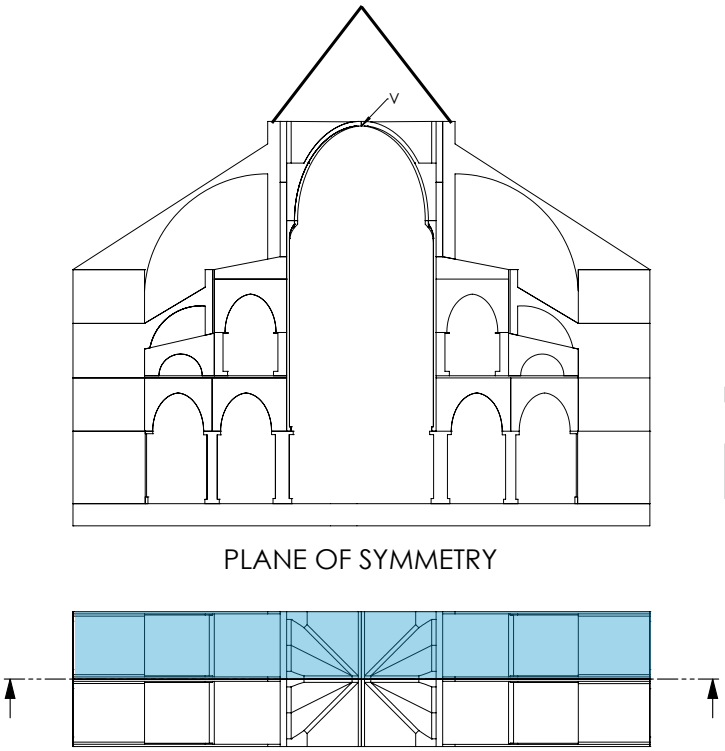

Figure 7: The part of the unit studied (highlighted in blue).

In Fig. 10 we show the total CPU time needed for the standard analyses in function of the number of elements, while in Fig. 11 we have plotted the same CPU time in function of the relative errors for the four quantities already represented in Fig. 9. In both the figures, the total CPU time is normalized with the CPU time of the finest mesh.

Looking at Figs. 9, 10 and 11, the choice of an average mesh size of 0.20 m seems a good balance between accuracy and calculation time. This is the mesh fineness that we have used in the calculations; as mentioned above, it has 1.83 millions of elements.

Parallel computing is used to decrease significantly the length of the analyses. All the simulations have been performed using a 24-cores workstation. The entire model is, thus, divided into 24 geometric domains, taking advantage of the 24 processors of the machine.

3 The material model

Masonry composed by ashlars and mortar joints can be modeled as a no-tension material: its tensile strength is so small that it can be considered as practically null, while the compressive strength is so high, usually greater than 40 MPa, that it is never attained in the body of the structure (normally, the highest compression in monumental structures is of the order of $4 \div 6$ MPa).

Hence, a suitable constitutive law must be used to model a continuum composed of ashlars and mortar-joints. Such a law should model the possibility of damage of the

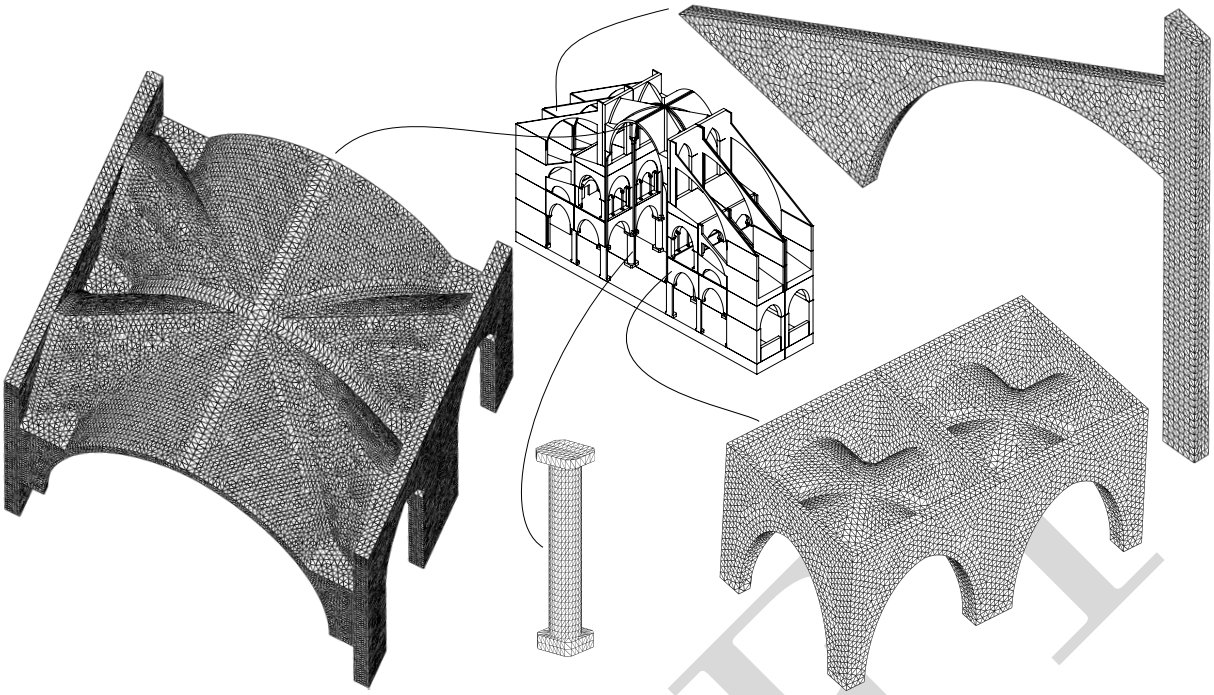

Figure 8: Details of the mesh used for the finite element analyses.

material, i.e. the formation of cracks due to tensile stresses. In our calculations, the following assumptions have been made to model the nonlinear behavior of stone structures, schematically represented in Fig. 12:

- in compression, the material is described by an isotropic linearly elastic constitutive law with infinite strength. This is a strong assumption, [Heyman, 1995], [Stefanou et al., 2015], but it is not expected to alter the results (as said above, compressions are always far below the admissible compressive stress);
- in tension, the material is assumed to be isotropic linearly elastic until the maximum principal stress does not exceed the tensile strength; a small, but not null, tensile strength σ_{max} is hence considered for the material;
- when the maximum principal stress exceeds the tensile strength σ_{max}, failure is modeled using a nonlinear constitutive law based on the softening model proposed by Hillerborg, Modéer and Petersson, [Hillerborg et al., 1976].

The Cathedral Notre Dame of Paris is built with ashlars of a limestone extracted from quarries of the Paris region. Not all the stones are from the same quarry, hence the mechanical characteristics of the material are not uniform throughout all the building. In addition, no certain data are available about the mechanical properties of the stone and of the mortar used by the constructors. That is why data derived from the literature have been used for the simulations.

An equivalent homogenized Young's modulus E_s, assuming that both stone and mortar-joints have the same Poisson's ratio, is derived from classical homogenization theory, see

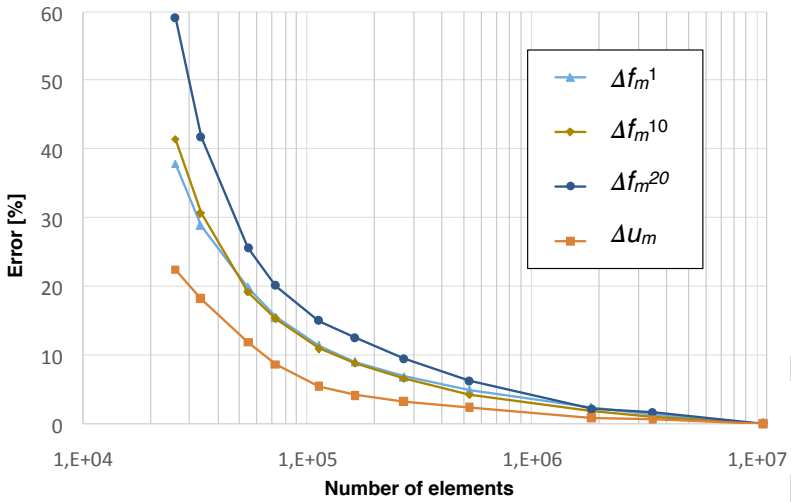

Figure 9: Relative error for three eigenfrequencies and the vertical displacement of point V as function of the elements number of each mesh m.

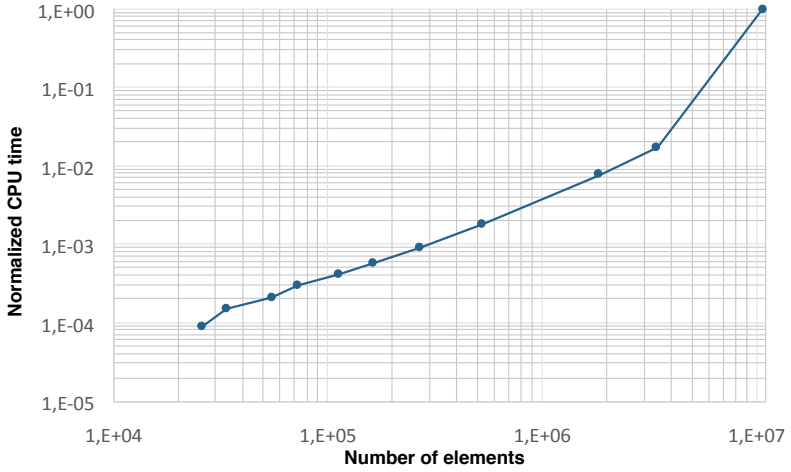

Figure 10: Normalized CPU times of the standard analyses versus the number of elements.

e.g. [Cecchi and Sab, 2002], [Como, 2013], namely

$$E_{eq} = \frac{E_m\,(1 + s/h_b)}{E_m/E_b + s/h_b}, \tag{2}$$

where E_b and E_m are the Young's moduli respectively of masonry blocks and mortar-joints, while h_b and s are the height of the blocks and thickness of the joints. Relying on the investigations made during a survey of the building, we can evaluate $h_b = 2.5 \times 10^{-1}$ m and $s = 1.0 \times 10^{-2}$ m. For mortar, a modulus $E_m = 2.5$ GPa is chosen, evaluated from modern hydraulic mortars, while for stone a modulus $E_b = 20$ GPa is selected, which is a mean value for limestone—for more details, see again [Como, 2013]. The resulting Young's modulus is $E_{eq} = 14.8$ GPa, thus a value $E_s = 14$ GPa is selected, for a matter of safety. The Poisson's ratio and the density are selected relying on typical values mentioned in the literature for limestone, namely:

$$\rho_s = 2000 \text{ kg/m}^3, \qquad \nu_s = 0.25.$$

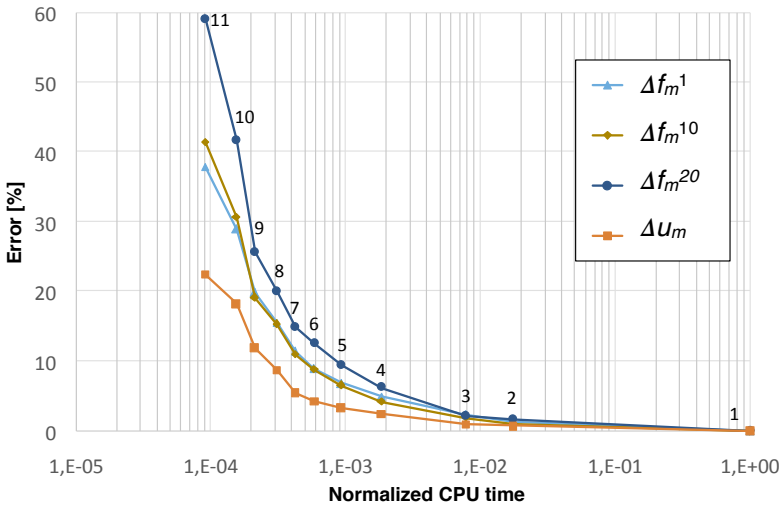

Figure 11: Normalized CPU times versus relative errors for three eigenfrequencies and the vertical displacement of point V; numbers 1 to 11 indicate the mesh m.

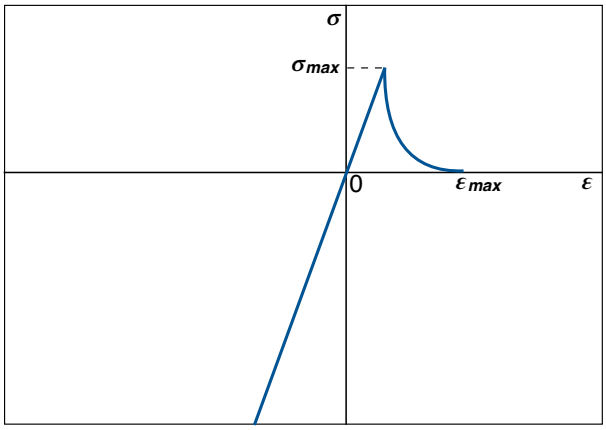

Figure 12: Constitutive law used for modeling the stone behavior

Damage, i.e. fracture produced by tensile stresses, is taken into account through the *brittle cracking* model of [Hillerborg et al., 1976]. In this model, a crack appears when the maximum principal stress over an element exceeds its tensile strength σ_{max}. The crack forms in the plane orthogonal to the direction of the principal stress exceeding the tensile limit, see also [Dassault Systèmes, 2016].

As far it concerns the propagation of the cracks, an energy criterion is used. This allows to minimize mesh dependency due to the softening behavior of the material and to dissipate adequately the energy. We have used a simplified law, shown in Fig. 13 to represent the behavior in Fig. 12: in tension, the elastic phase is followed by a piecewise linear softening one, representing the damage of the material.

The fracture energy for normal tensile stresses is defined as, see Fig. 13 a):

$$G_f = G_f^1 + G_f^2 + G_f^3 = \int_0^{w_0} \sigma \, dw + \int_{w_0}^{w_k} \sigma \, dw + \int_{w_k}^{w_f} \sigma \, dw, \tag{3}$$

where σ is the maximum principal stress; w is the displacement normal to the crack surface, defined as the product of the normal strain ε and a characteristic length h, i.e.

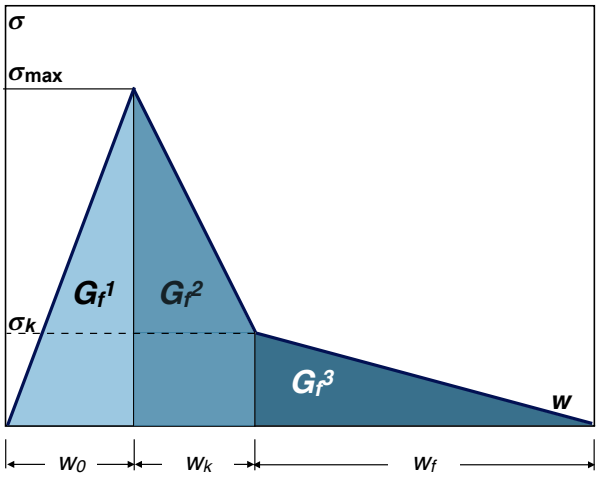

Figure 13: Representation of the tensile softening law used in the calculations.

$w = \varepsilon h$; w_0 is the normal displacement corresponding to σ_{max}, w_k that relative to the kink point and w_f the one corresponding to the complete loss of strength.

Because the assumed constitutive law is piecewise linear, putting

$$\Psi = \frac{\sigma_k}{\sigma_{max}}, \quad \zeta = \frac{w_k}{w_f}, \tag{4}$$

the three integrals in eq. (3) become

$$\begin{aligned} G_f^1 &= \int_0^{w_0} \sigma \, dw = \frac{\sigma_{max} w_0}{2} = \frac{\sigma_{max}^2}{2E_s} h, \\ G_f^2 &= \int_{w_0}^{w_k} \sigma \, dw = \frac{\sigma_{max}}{2}(1+\Psi)(\zeta w_f - \frac{\sigma_{max}}{E_s} h), \\ G_f^3 &= \int_{w_k}^{w_f} \sigma \, dw = \frac{\sigma_{max}}{2}\Psi(1-\zeta) w_f, \end{aligned} \tag{5}$$

so that

$$G_f = \frac{\sigma_{max}}{2}\left[(\Psi+\zeta) w_f - \Psi h \frac{\sigma_{max}}{E_s}\right]. \tag{6}$$

For masonry, relying on the experimental results from uniaxial tensile tests on specimens with a characteristic length $h = 100$ mm, [van der Pluijm, 1999], the following parameters have been chosen

$$\sigma_{max} = 0.73 \text{ MPa}, \qquad G_f = 11.3 \text{ N/m}.$$

Using these values, we get the value of w_f (Ψ and ζ must be fixed; in the simulations, we have put $\Psi = 1/3$ and $\zeta = 1/2$):

$$w_f = \frac{1}{\Psi+\zeta}\left(\frac{2G_f}{\sigma_{max}} + \Psi h \frac{\sigma_{max}}{E_s}\right), \tag{7}$$

whose value is automatically calculated for each element by *ABAQUS*; for instance, for $h = 100$ mm we get $w_f = 5.2 \times 10^{-2}$ mm.

4 The wind model

We are concerned here with the determination of the critical wind speed that the Cathedral can withstand, i.e. we are not interested in calculating the response to wind of the Cathedral as a civil structure to be designed. To this purpose, we need a model of the wind phenomenon as close as possible to the real physical phenomenon. That is why we can completely discard norms and in particular the somewhat troubling and rather confusing Eurocode 1.

The wind close to the Earth surface is just what happens in the boundary layer of the flow of air masses. As such, we need a law describing the variation of the wind speed v with the distance z from the ground typical of what happens in a boundary layer: a null speed at $z = 0$ and a decreasing gradient $dv(z)/dz$.

Actually, the wind speed is not exactly null at the ground level and, mainly for the ruggedness of the surface, it is practically constant until a certain height z_0. Above z_0, $v(z)$ increases more and more slowly.

There are two types of laws commonly used for modeling the wind vertical profile: a power law and a logarithmic law, [Sachs, 1978]. For instance, in [Coccia et al., 2015] a power law is used in the form (p stands for power law)

$$\eta_p = \zeta^\alpha, \tag{8}$$

where we have introduced the two dimensionless variables

$$\eta = \frac{v}{v_0}, \quad \zeta = \frac{z}{z_0}, \tag{9}$$

with z_0 the reference height, where the wind speed v_0 is known, and α an exponent, put equal to 0.35 in [Coccia et al., 2015], value suggested for urban areas. Taking into account the skyline of Paris, we have chosen for z_0 the value of 10 m.

The logarithmic velocity distribution is based on reasonable physical considerations of uniform shear stress within the first few meters of elevation and a mixing length that increases linearly above the mean free surface. To the equation of a logarithmic profile different forms can be given, but if we want that $v = 0$ for $z = 0$ and $v = v_0$ for $z = z_0$, like the power law, a suitable expression is (ℓ stands for logarithmic law)

$$\eta_\ell = \ln\left[1 + (e - 1)\zeta\right]. \tag{10}$$

The converse equations of eqs. (8) and (10) are respectively

$$\zeta = \eta_p^{\frac{1}{\alpha}} \tag{11}$$

and

$$\zeta = \frac{e_\ell^\eta - 1}{e - 1}; \tag{12}$$

they are traced in Fig. 14, with $\alpha = 0.35$ for the power law, where the wind profile is constant until the height z_0 (i.e. $\zeta = 1$) for the assumption of uniform wind speed for $z \leq z_0$ introduced above.

As it is apparent, the power law underestimates the logarithmic law; nevertheless, it is important to point out that the power law strongly depends upon the coefficient α. For instance, for $\alpha = 0.5$ eqs. (8) and (10) give practically the same diagram of $\eta(\zeta)$. The advantage of eq. (10) is that it is not sensitive to coefficients like α, that are delicate to be determined for each case.

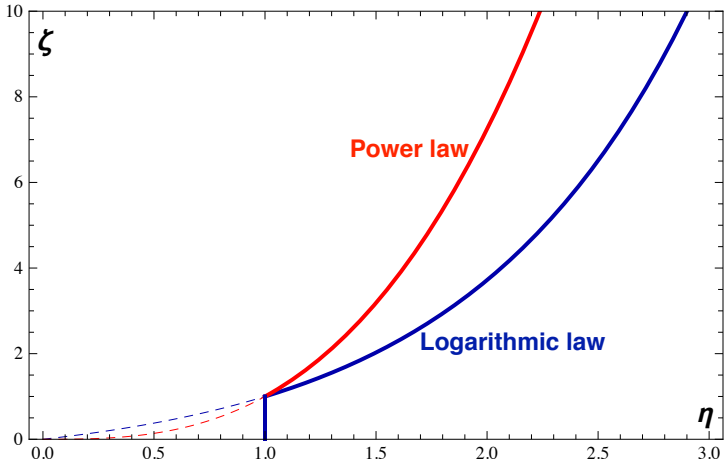

Figure 14: Wind speed profiles.

The wind pressure p is obtained as a drag force per unit of exposed surface using the relation

$$p = \frac{1}{2} C_D \, \rho \, v^2, \tag{13}$$

where ρ is the mass density of air, $\rho = 1.225$ kg/m^3 at an ambient temperature of 15°C, and C_D is the drag coefficient. Its value mainly depends upon the Reynolds number, the form and exposition of the surface impinged by wind, besides its ruggedness and other parameters, like the Mach and Froude numbers etc.

In the case of a surface like the side of the Cathedral Notre Dame, it is impossible to have a global value of C_D without preliminary tests in a wind tunnel. Because this has not been possible, we have evaluated C_D in the following way: we have considered the side of Notre Dame as a vertical rectangular plate, whose total height is $z_1 = 45$ m, the height of the roof top. Though the height between 35 and 45 m, the zone occupied by the roof, is actually an inclined plate, we have considered it, conservatively, as vertical. The effect of decorations, pinnacles, flying buttresses and so on, cannot be evaluated, but they are likely to increase the value of C_D.

Then, the values given in the literature for a rectangular plate perpendicular to the flow are:

- $C_D = 1.28$ for a rectangular plate in a 3D flow;
- $C_D = 1.98 \div 2.05$ for a rectangular plate in a 2D flow, i.e. for an infinitely long plate.

Because of the uncertainties affecting the evaluation of C_D, we have considered two values for C_D:

- a lower value $C_D^{min} = 1.28$, as if the lateral surface of the unit in Fig. 1 were an isolated rectangular plate;
- an upper value $C_D^{max} = 2$, because the Cathedral is very long, 130 m, with respect to the width of half the lateral unit in Fig. 1, 6 m, so that it can be approximatively considered that the flow impinging the unit is close to a 2D flow.

R. Mark, [Mark, 1982], gives the distribution of C_D in Fig. 15. It has been derived by experimental measures in wind-tunnel tests conducted at the Universities of Iowa, [Chien et al., 1951], and of Toronto, [Davenport, 1967], though not specifically on geometries like those typical of a Gothic Cathedral. Such a distribution shows that C_D can considerably vary, and it attains average values ranging from ~ 1 to ~ 1.8. Nevertheless, it is worth recalling that Mark uses the formula

$$p = \frac{1}{2}\rho C_D \; G \; v^2 \tag{14}$$

to determine the wind pressure, where G is a coefficient called *gust factor*, to account for the dynamic effects of the wind pressure. In his calculation of the wind effects on the Cathedral of Amiens, Mark takes the value $G = 2.3$, which gives a product $C_D G$ varying from ~ 2.3 to ~ 4.14. Finally, we remark that in [Coccia et al., 2015] the evaluation given for the wind pressure corresponds to put, on the whole, $C_D = 1.5$.

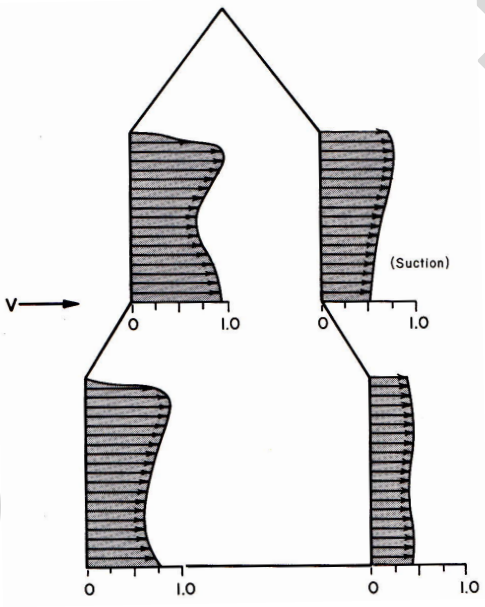

Figure 15: Distribution of C_D on a Gothic-Gathedral, according to [Mark, 1982].

Because of the uncertainties intrinsically linked to the determination of the wind and of C_D, our approach has been that of beginning by bounding the critical wind speed between lower and upper bounds. We have hence considered, for each wind speed v used for calculations, two wind pressures:

- a lower bound pressure, determined using the power law (8) for the wind profile and $C_D = C_D^{min}$:

$$p_{min} = \frac{1}{2}\rho \; C_D^{min} v_0^2 \eta_p^2; \tag{15}$$

- an upper bound pressure, found using the logarithmic law (10) for the wind profile and $C_D = C_D^{max}$:

$$p_{max} = \frac{1}{2}\rho\ C_D^{max} v_0^2 \eta_\ell^2. \tag{16}$$

This approach allows to obtain a reasonable estimation of the wind pressure bounds for any wind speed.

It is worth to give the pressure distribution (13) in a dimensionless form. To this end, let us introduce the pressure p_0, corresponding to the value of the wind speed v_0:

$$p_0 = \frac{1}{2} C_D\ \rho\ v_0^2. \tag{17}$$

Then, the dimensionless value π of the pressure is obtained as

$$\pi = \frac{p}{p_0} = \eta^2, \tag{18}$$

which gives the dimensionless form of eqs. (15) and (16):

$$\begin{aligned} \pi_{min}(\zeta) &= \zeta^{2\alpha}, \\ \pi_{max}(\zeta) &= \ln^2\left[1 + (e-1)\zeta\right]. \end{aligned} \tag{19}$$

The converse of functions (19),

$$\begin{aligned} \zeta(\pi_{min}) &= \pi_{min}^{\frac{1}{2\alpha}}, \\ \zeta(\pi_{max}) &= \frac{e^{\sqrt{\pi_{max}}} - 1}{e-1}, \end{aligned} \tag{20}$$

are represented in Fig. 16. It is apparent that for $\zeta > 1$, i.e. for $z > z_0$, $\pi(\zeta)$ is almost linear in both the cases.

In order to simplify the calculations, without altering the overall wind action, we have adopted a load profile constant piecewise, indicated in Fig. 16:

- $\pi(\zeta) = \pi_0 = 1$ for $\zeta \leq 1$, i.e. $p = p_0$ for $z \leq z_0$;
- $\pi(\zeta) = \pi_1^{min}$ or $\pi(\zeta) = \pi_1^{max}$ for $\zeta_0 < \zeta \leq \zeta_1$, i.e. $p = p_1^{min}$ or $p = p_1^{max}$ for $z_0 < z \leq z_1$,

where

$$\zeta_1 = \frac{z_1}{z_0} = 4.5, \tag{21}$$

$$\pi_1^{min} = \frac{1}{\zeta_1 - 1}\int_1^{\zeta_1} \zeta^{2\alpha} d\zeta = \frac{1}{1+2\alpha}\frac{\zeta_1^{1+2\alpha} - 1}{\zeta_1 - 1} \simeq 2, \tag{22}$$

$$\begin{aligned} \pi_1^{max} =& \frac{1}{\zeta_1 - 1}\int_1^{\zeta_1} \ln^2\left[1 + (e-1)\zeta\right] d\zeta = \\ & \frac{\left[1 + (e-1)\zeta_1\right]\left\{\left[\ln(1 + (e-1)\zeta_1) - 1\right]^2 + 1\right\} - e}{(e-1)(\zeta_1 - 1)} \simeq 2.98, \end{aligned} \tag{23}$$

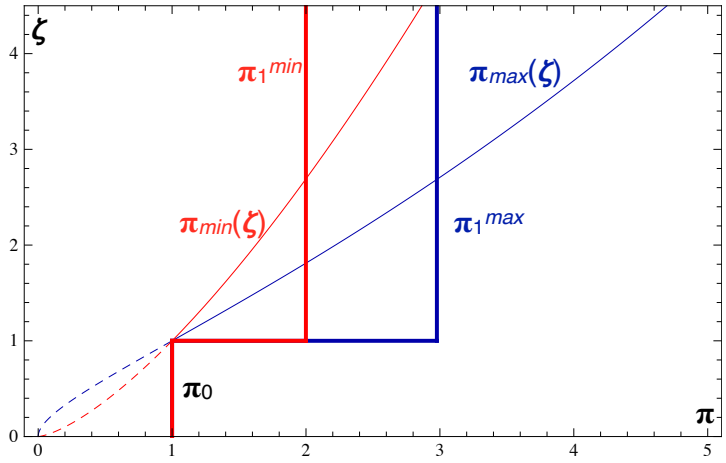

Figure 16: Wind pressure profiles.

and hence

$$\begin{aligned} p_1^{min} &= \pi_1^{min}\ p_0^{min} = \frac{1}{2}\pi_1^{min}\ C_D^{min}\ \rho\ v_0^2, \\ p_1^{max} &= \pi_1^{max}\ p_0^{max} = \frac{1}{2}\pi_1^{max}\ C_D^{max}\ \rho\ v_0^2. \end{aligned} \tag{24}$$

To remark that the value of π_1 depends exclusively upon the ratio ζ_1. Such a wind pressure profile, less strong in the upper part, allows to take into account, indirectly, for the slope of the roof, that is likely to reduce the value of C_D.

The values of p_0 and p_1 are the overall wind action on the Cathedral. Nevertheless, this action is distributed partly on the windward side and partly on the leeward side. Considering the experimental diagram of C_D in Fig. 15 and following what done in [Como, 2013] and [Coccia et al., 2015], we consider a leeward side (suction) load half of the windward one, i.e.

$$p = p_w + p_\ell, \quad p_w = 2p_\ell \ \Rightarrow\ p_w = \frac{2}{3}p, \quad p_\ell = \frac{1}{3}p, \tag{25}$$

where p_w indicates the windward pressure load and p_ℓ the leeward one. In Fig. 17 we show a scheme of the wind loading on the Cathedral.

5 The numerical method

The basic idea for the evaluation of the wind strength of the Cathedral is to control the horizontal displacement of the upper part of the Cathedral, identified conventionally with that of point V. For a given value of the wind pressure, such a displacement is calculated. The wind strength of the Cathedral is then identified with the wind speed that produces an unbounded displacement of point V.

In fact, because the constitutive law is nonlinear and it describes also the damage produced by tensile stresses, the structure of the Cathedral will have a nonlinear response to wind

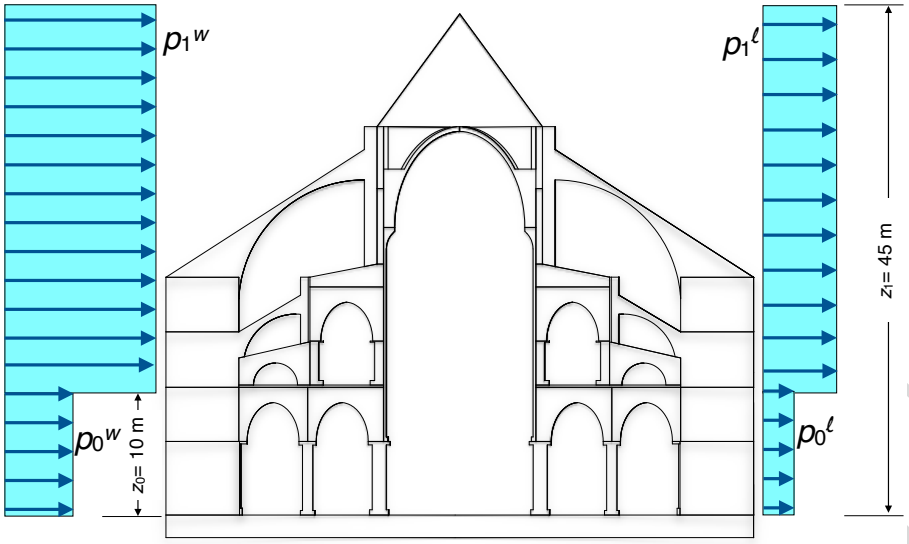

Figure 17: Wind loading on the Cathedral.

and a damage will appear for a sufficiently great value of the wind pressure. Such a damage, cracks propagating into the structure, will increase with the wind pressure, until a point where it will be so extended throughout the structure that a ruin mechanism will be formed. At that point, the structure will not be anymore able to withstand the wind loads and the displacement of V will progress indefinitely with time, i.e. it will be unbounded.

To take into account for the stress distribution produced by the own weight of the Cathedral, an implicit static analysis is previously done. The resulting configuration is then used as the starting point for a subsequent nonlinear explicit analysis, in which the wind loads described in Sect. 4 are applied in a quasi-static manner. A mass proportional damping is assumed in order to reach equilibrium rapidly and to dissipate unwanted oscillations (quasi-static condition).

As mentioned above, the simulations are done applying the load smoothly in time. The values of the wind pressures p_0 and p_1, are multiplied by a factor $A(t)$ that varies from $A_0 = 0$, for $t = 0$, to $A_f = 1$, for $t \geq t_f$; different choices are possible to have a smooth variation of $A(t)$, we have put

$$A(t) = \begin{cases} A_0 + (A_f - A_0)\,\xi^3\left(10 - 15\xi + 6\xi^2\right) & \text{if } 0 \leq t < t_f, \\ 1 \quad \text{if } t \geq t_f, \end{cases} \tag{26}$$

where

$$\xi = \frac{t - t_0}{t_f - t_0}. \tag{27}$$

The diagram of $A(t)$ is shown in Fig. 18. After t_f, the load conserves indefinitely the same maximum value.

The incremental analysis allows to obtain the response curve of the structure, i.e. the curve displacement of V versus time, for any value of the wind speed. If the structure reaches an equilibrium configuration under the applied wind pressure, the response curve

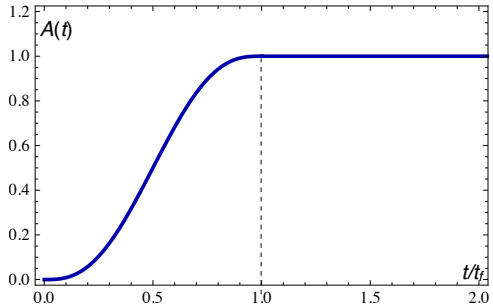

Figure 18: The diagram of factor $A(t)$.

reaches an horizontal asymptote, indicating that the horizontal displacement has come to a value that remains constant under the wind action.

On the contrary, when the Cathedral reaches its ultimate state, the response curve diverges, due to the fact that the structure has failed: cracks have formed a collapse mechanism.

6 Structural calculations

6.1 Bounding the critical wind speed

We have executed wind analyses for different wind speeds. The wind speed taken as reference is v_0, i.e. the speed at 10 m above the ground level. In Tab. 3 we give, as functions of v_0, the corresponding values of p_0^{min}, p_1^{min}, p_0^{max} and p_1^{max}, along with the wind speed at 45 m according to the power law, v_{45}^p, and to the logarithmic one, v_{45}^ℓ.

Table 3: Wind speeds at $z = 10$ m, corresponding wind pressures min and max and wind speeds at $z = 45$ m.

	$C_D^{min},\ \eta = \eta^p$			$C_D^{max},\ \eta = \eta^\ell$		
v_0 [km/h]	p_0^{min} [kPa]	p_1^{min} [kPa]	v_{45}^p [km/h]	p_0^{max} [kPa]	p_1^{max} [kPa]	v_{45}^ℓ [km/h]
80	0.387	0.774	135.4	0.605	1.801	173.4
100	0.605	1.209	169.3	0.945	2.814	216.7
120	0.871	1.742	203.1	1.361	4.052	260.0
140	1.186	2.371	237.0	1.853	5.515	303.4
160	1.549	3.096	270.9	2.420	7.204	346.7
170	1.748	3.495	287.8	2.732	8.132	368.4
180	1.960	3.919	304.7	3.063	9.117	390.0
200	2.420	4.838	338.6	3.781	11.256	433.4
220	2.928	5.854	372.4	4.575	13.619	476.7
240	3.484	6.967	406.3	5.444	16.208	520.1
250	3.781	7.559	423.2	5.908	17.587	541.7
260	4.089	8.176	440.1	6.390	19.022	563.4

For each wind speed, we have hence done two calculations: one for the couple $(p_0^{min},\ p_1^{min})$ and the other one for the couple $(p_0^{max},\ p_1^{max})$, and we have searched the non-linear response of the Cathedral, in terms of horizontal displacement of point V. For the two series of wind loads, the minimum and the maximum, we find a critical wind pressure couple, $(p_0^{min},\ p_1^{min})_{crit}$ and $(p_0^{max},\ p_1^{max})_{crit}$. From them, through eq. (17) we obtain respectively v_{0crit}^{max} and v_{0crit}^{min}, i.e. the upper and lower bound for the critical wind speed, conventionally measured at 10 m above the ground level, that the Cathedral can withstand.

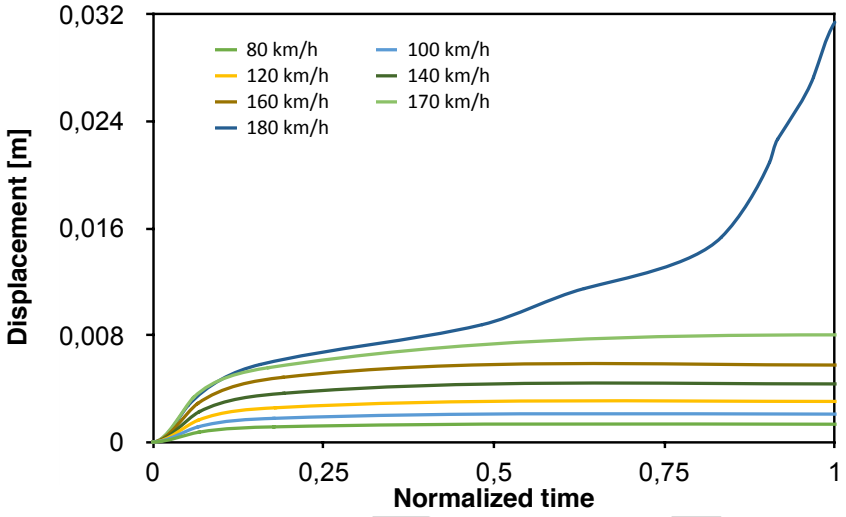

Figure 19: Diagrams time-displacement: C_D^{min} and $\eta = \eta^p$.

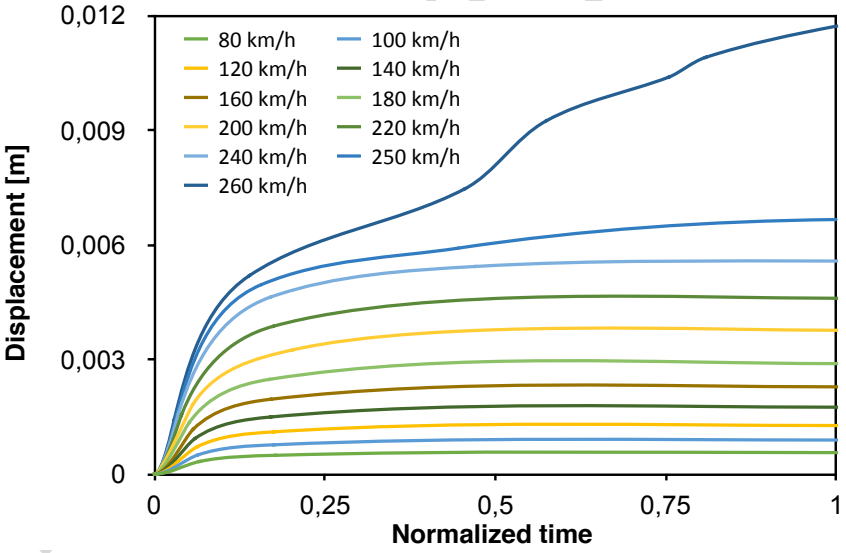

Figure 20: Diagrams time-displacement: C_D^{max} and $\eta = \eta^\ell$.

The results of the calculations are shown in Figs. 19 to 21 and in Tab. 4. It is evident that for the case C_D^{min} and the power law for the wind speed profile, the critical velocity is $v_0 = 260$ km/h. In fact, the diagram of the displacement diverges with time: the displacement increases with the duration of the simulation. This is the sign that the structure has been transformed into a mechanism by the propagation of the cracks. For the same reasons, in the case of C_D^{max} and the logarithmic law, the critical speed is $v_0 = 180$

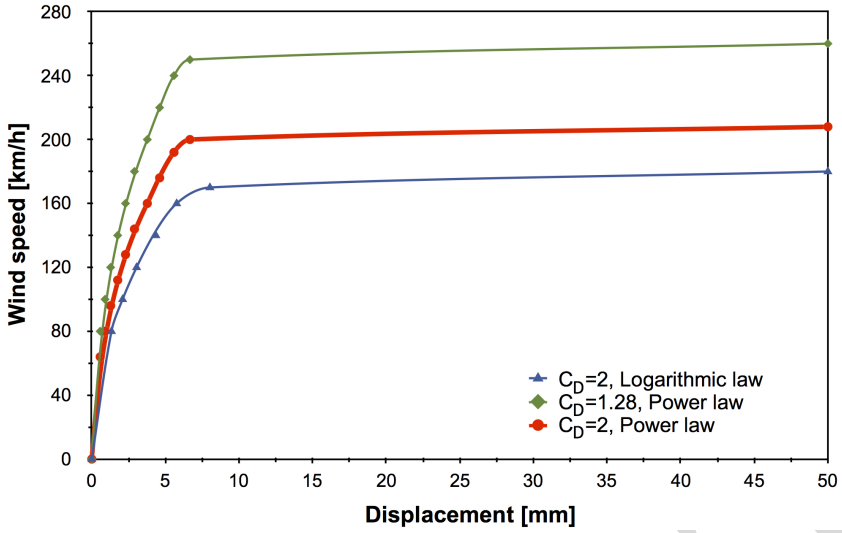

Figure 21: Diagrams displacement-wind speed.

km/h. Hence, the lower bound for the critical wind speed is $v_{0crit}^{min} = 180$ km/h and the upper one is $v_{0crit}^{max} = 260$ km/h.

In Tab. 4, we show, for each wind speed, δV_{max}, i.e. the maximum horizontal displacement of point V. We have indicated the ultimate displacement as ∞, because for the critical wind speed δV_{max} is unbounded. However, to trace the diagrams in Fig. 21, the ultimate displacements have been taken conventionally equal to 50 mm.

Table 4: Wind speeds at $z = 10$ m and corresponding horizontal displacements of point V for the two cases C_D^{min}, $\eta = \eta^p$ and C_D^{max}, $\eta = \eta^\ell$.

v_0 [km/h]	δV_{max} [mm]	
	C_D^{min}, $\eta = \eta^p$	C_D^{max}, $\eta = \eta^\ell$
80	0.6	1.3
100	0.9	2.1
120	1.3	3.0
140	1.8	4.4
160	2.3	5.8
170	2.6	8.0
180	2.9	∞
200	3.8	-
220	4.6	-
240	5.6	-
250	6.7	-
260	∞	-

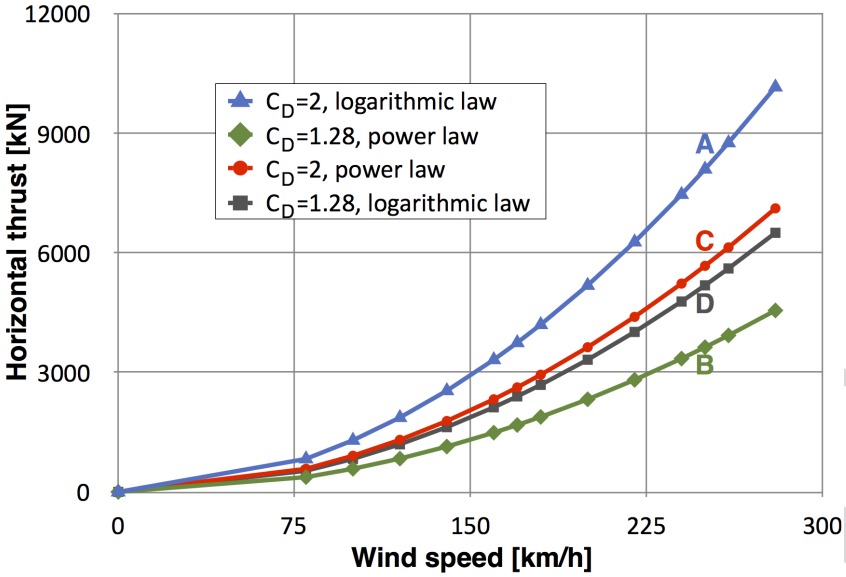

Figure 22: Diagrams of the total wind thrust.

6.2 Evaluation of the critical wind speed

The critical interval for the wind speed has an amplitude of 80 km/h. For better approaching the true value of the critical wind speed, we can consider the diagrams in Fig. 22. Here, we have plotted the total wind thrust as a function of the wind speed. The upper and lower curves correspond to the cases presented in Tab. 3, and are denoted in Fig. 22 as curves A and B, respectively.

The intermediate curves have been traced considering the power law with C_D^{max}, curve C, and the logarithmic law with the value C_D^{min}, curve D. These two curves are very close, and located practically in the middle of the zone delimited by the bounding curves A and B: curve C corresponds to the 97% of the mean of A and B, i.e. $C = 0.97(A + B)/2$, while curve D to the 88%, i.e. $D = 0.88(A + B)/2$. The values of the total wind thrust H_w for the four curves above are given in Tab. 5.

The true value of C_D is likely to be closer to C_D^{max} than to C_D^{min}, so the best estimation of a representative real value of the wind thrust is given by curve C: $C_D = C_D^{max} = 2$ and a wind profile described by a power law, $\eta = \eta^p$.

Through eq. (13), we see easily that the diagram displacement-wind speed for this case, $C_D = 2$ and $\eta = \eta^p$, can be obtained, without any additional computation, simply scaling the wind speed:

$$v_0^C = v_0^B \sqrt{\frac{C_D^B}{C_D^C}} = v_0^B \sqrt{\frac{1.28}{2}} = 0.8\ v_0^B, \tag{28}$$

where v_0^B denotes the wind speed for the case of curve B in Fig. 22, i.e. for $C_D = 1.28$ and $\eta = \eta^p$, while v_0^C is the wind speed for the case of curve C in Fig. 22, i.e. for $C_D = 2$ and $\eta = \eta^p$. Of course, this result has been obtained keeping constant the value of the wind pressure for the same wind profile, the power law. By consequence, for each value of the wind pressure the only thing that changes is just the wind speed, to be rescaled

Table 5: Overall wind thrusts H_w on the Cathedral.

v_0 [km/h]	Overall wind thrust H_w [kN]			
	Curve A $C_D^{max},\ \eta = \eta^\ell$	Curve B $C_D^{min},\ \eta = \eta^p$	Curve C $C_D^{max},\ \eta = \eta^p$	Curve D $C_D^{min},\ \eta = \eta^\ell$
80	829	372	581	531
100	1295	581	907	829
120	1865	836	1306	1194
140	2539	1138	1778	1625
160	3316	1486	2322	2122
170	3743	1678	2622	2396
180	4197	1881	2939	2686
200	5181	2322	3629	3316
220	6269	2810	4391	4012
240	7461	3344	5225	4775
250	8095	3629	5670	5181
260	8756	3925	6132	5604
280	10155	4552	7112	6499

through eq. (28). The complete set of results for $C_D = 2$ and $\eta = \eta^p$ is reported in Tab. 6 while the corresponding curve displacement-wind speed is still traced in Fig. 21.

Considering these results, it appears that the collapse of the Cathedral is likely to happen for a wind speed

$$v_{0crit} \sim 208 \text{ km/h}.$$

For such a value of v_0, we get, see Tab. 6, a velocity of the wind at the height of 45 m above the ground level, i.e. at the top of the Cathedral,

$$v_{45}^p \sim 352 \text{ km/h}$$

for the profile $\eta = \eta^p$ of the wind velocity (power law).

Such a meteorological event is very improbable: the highest wind speed ever recorded in France is just of 360 km/h, on November 1^{st} 1968, at the top of Mont Aigoual, i.e. at 1567 m above the sea level, much more than 45 m. This means that the structural collapse of Notre Dame of Paris as the consequence of a wind storm is a very unlikely event.

6.3 The mechanism of structural collapse

The numerical simulations described above allows to follow the diffusion of the damage in the structure, which leads to the formation, for the critical wind speed v_{0crit}, of the collapse mechanism. At this stage, in fact, the damage has reached such a diffusion that a mechanism is formed, leading to the failure of the structure, as already explained.

The phases of the structural collapse are shown in Fig. 23; for different wind speeds v_0, the deformation of the structure and the propagation of the cracks is shown.

Table 6: Data for $C_D = 2$ and $\eta = \eta^p$.

v_0 [km/h]	p_0 [kPa]	p_1 [kPa]	v_{45}^p [km/h]	H_w [kN]	δV_{max} [mm]
64	0.605	1.209	108.3	581	0.6
80	0.945	1.890	135.4	907	0.9
96	1.361	2.721	162.5	1306	1.3
112	1.853	3.704	189.6	1778	1.8
128	2.420	4.838	216.7	2322	2.3
144	3.063	6.123	243.8	2939	2.9
160	3.781	7.559	270.9	3629	3.8
176	4.575	9.147	297.9	4391	4.6
192	5.444	10.885	325.0	5225	5.6
200	5.908	11.811	338.6	5670	6.7
208	6.390	12.775	352.1	6132	∞

As it was to be expected, the failure occurs when the flying buttresses are severely damaged by the wind thrust; the clearstorey can then rotate after the formation of four *plastic hinges*, produced by the propagation of cracks, in the high vault and at the base of the same clearstorey. The cracks propagating, also the massive buttresses are damaged and collapse. Large cracks appear also in the vaults of the lateral aisles.

It is interesting to highlight the collapse of the high sexpartite vault, depicted in Fig. 24. The plastic hinges on the vault deserve a particular consideration: they are more or less longitudinal, though they are not produced over a cylindrical surface, like a barrel vault, but on a sexpartite ribbed vault. So, the location of the plastic hinges in the vault is confirmed, by a 3D model, to be similar to that often used in a 2D scheme.

The total estimated weight of the Cathedral unit, highlighted in red in Fig. 1, is $W_{tot} = 60300$ kN; so the ratio with the horizontal wind thrust that causes the structural collapse is

$$\frac{W_{tot}}{H_w} = 60300/6132 \sim 9.8.$$

For comparison, the ratio calculated by R. Mark for Amiens is almost the double: 18.7, [Mark, 1982]. This is due to two main reasons: the evaluation made by R. Mark cannot be considered as that corresponding to the structural collapse and the height of the Amiens Cathedral, 54 m, is greater than that of Paris, 45 m, so a lesser wind thrust is sufficient for causing the structural failure.

However, it is worth noting that, though the wind speed v_{0crit} is highly improbable, since $v_0 = 160$ km/h a damage appears in the structure, see Fig. 23, in the form of cracks. Hence, though the global failure of the Cathedral under the action of the wind is really unlikely, winds that can actually produce non negligible damages to the structure of the Cathedral are really possible. As said in the Introduction, in December 1999, a wind speed of 169 km/h has been recorded inside Paris.

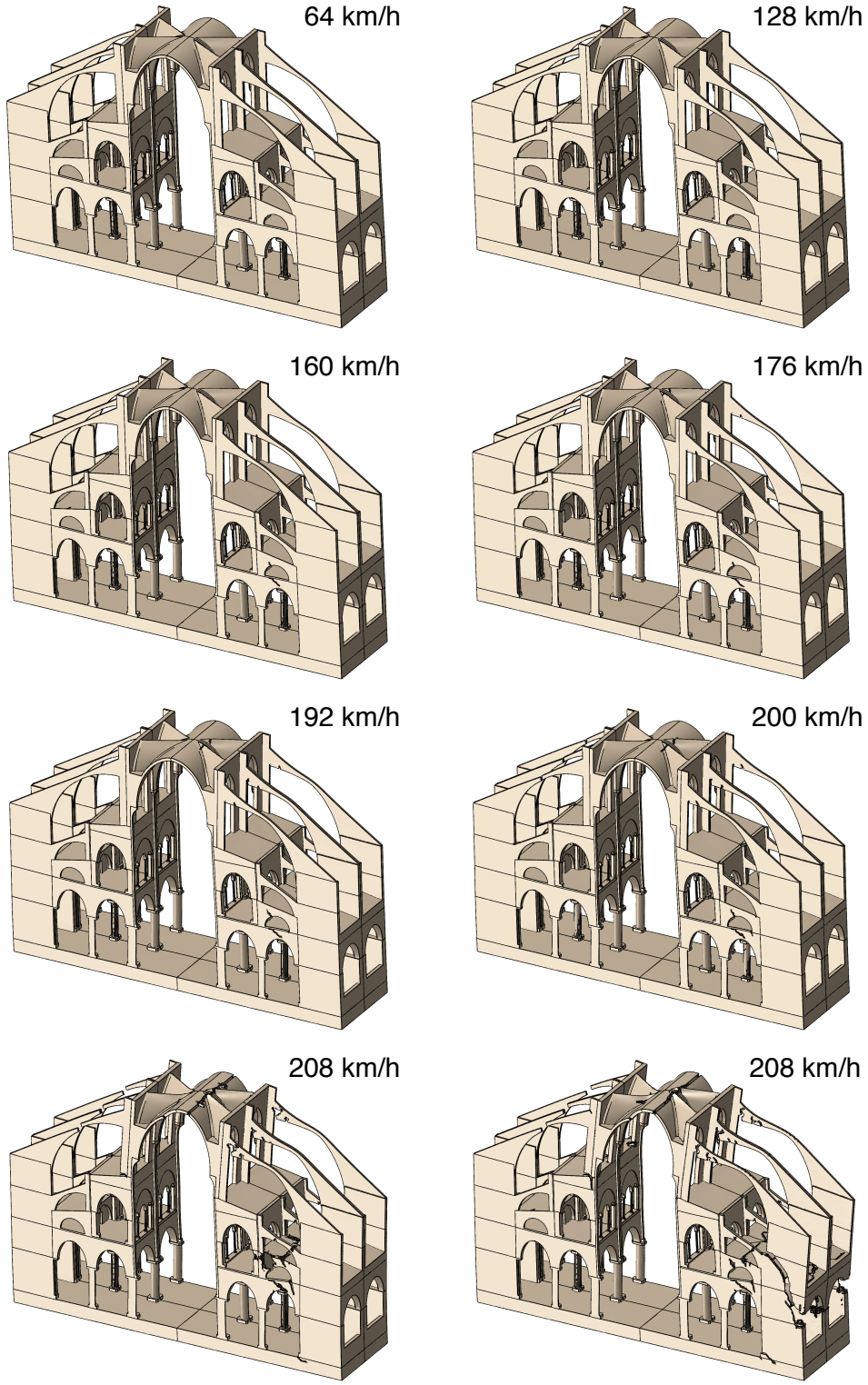

Figure 23: Progressive damage of the structure and formation of the collapse mechanism; the two last plots are for the same wind speed, but taken at two successive instants ($C_D = 2,\ \eta = \eta^p$).

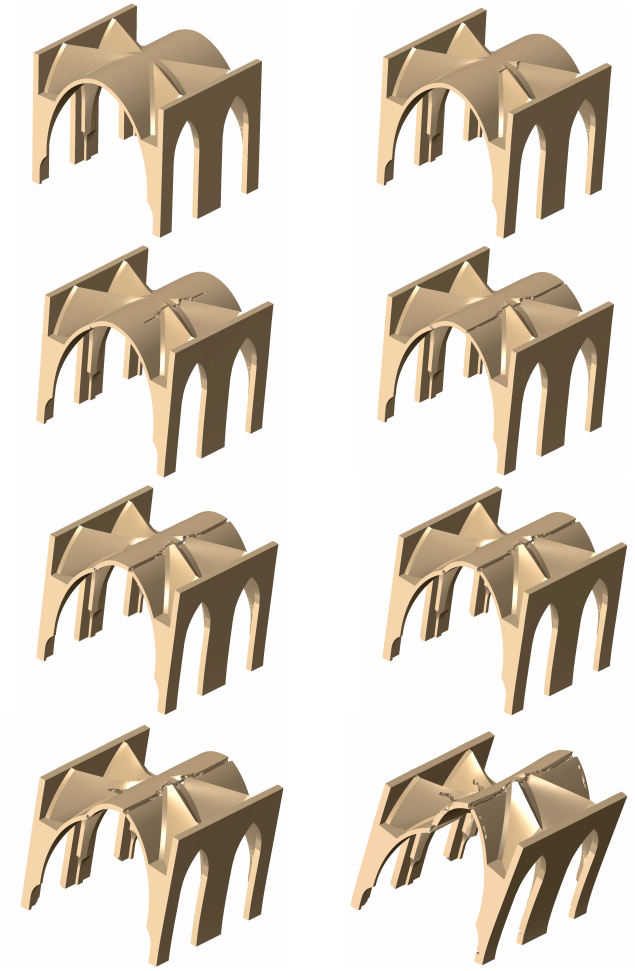

Figure 24: Progressive failure of the high sexpartite vault

7 Conclusion

The numerical simulations have clearly shown that severe wind storms are able to damage the structure of the Cathedral Notre Dame of Paris, but that a global structural failure is highly improbable.

Of course, we have just considered in this study the global collapse of the Cathedral. However, partial, though important, local damages can be produced in different parts of the Cathedral, like the pinacles, the timber spire, the roses, the flying buttresses, the same timber roof. It is not excluded that local important effects can be produced by phenomena like vortex shedding, while the roof could be lifted up or overthrown by the wind.

All these phenomena, that could happen also for wind speeds $v_0 < v_{0crit}$, should be studied apart and cannot be predicted with the approach followed in this paper, conceived to determine the overall strength to wind thrust and that has however different advantages. Namely, it allows to follow the progressive failure of the structure under increasing wind

speed and also to determine its true collapse mechanism, which should really difficult to be done on a Cathedral like Notre Dame, composed by five aisles and galleries, using a classical approach of limit analysis *à la Heyman*, like in [Coccia et al., 2015].

References

A. Cecchi and K. Sab. A multi-parameter homogenization study for modeling elastic masonry. *European Journal of Mechanics - A/Solids*, 21:249–268, 2002.

N. Chien, Y. Feng, H. H. Want, and T. T. Siao. Wind tunnel studies of pressure distribution on elementary building forms. Technical report, Institute of Hydraulics Research, University of Iowa, Ames, Iowa, 1951.

S. Coccia, M. Como, and F. Di Carlo. Wind strength of Gothic Cathedrals. *Engineering Failure Analysis*, 55:1–25, 2015.

M. Como. *Statics of historic masonry constructions*. Springer Verlag, Berlin, Germany, 2013.

Dassault Systèmes. Abaqus analysis user's guide. Technical Report Abaqus 6.14 Documentation, Simulia Corp., 2016.

A. G. Davenport. The treatment of wind loads on tall buildings. In A. Coull and B. Stafford Smith, editors, *Tall Buildings*. Pergamon Press, New York, 1967.

P. Frankl. *Gothic architecture*. Pelican History of Art. Penguin Books, Baltimore, Maryland, 1963.

J. Heyman. *The stone skeleton*. Cambridge University Press, Cambridge, UK, 1995.

A. Hillerborg, M. Modéer, and P. E. Petersson. Analysis of crack formation and crack growth in concrete by means of fracture mechanics and finite elements. *Cement and Concrete Resistance*, 6:773–782, 1976.

H. Jantzen. *Kunst der Gotik*. Rowohlt Taschenbuch Verlag, Hamburg, Germany, 1957.

R. Mark. *Experiments in gothic structure*. MIT Press, Cambridge, Massachussets, 1982.

R. Mark. *High gothic structure - A technological reinterpretation*. Princeton University Press, Princeton, New Jersey, 1984.

P. Sachs. *Wind forces in engineering*. Pergamon Press, Oxford, UK, 1978.

O. Von Simson. *The Gothic Cathedral*. Princeton University Press, Princeton, New Jersey, 1962.

I. Stefanou, K. Sab, and J.-V. Heck. Three dimensional homogenization of masonry structures with building blocks of finite strength: A closed form strength domain. *International Journal of Solids and Structures*, 54:258–270, 2015.

A. Tallon. La Cathédrale de Paris, 2010. URL `http://faculty.vassar.edu/antallon/ndp/vr/ndp_fr.html`.

G. G. Ungewitter. *Lehrbuch der Gotischen Konstruktionen.* T. O. Weigel Nachfolger, Leipzig, Germany. Available at Biblioteca Meccanico Architettonica: http://www.bma.arch.unige.it, 1890.

R. van der Pluijm. *Out-of-Plane bending of Masonry. Behavior and Strength.* Technische Universiteit Eindhoven, Eindhoven, The Netherlands, 1999.

C. Wilson. *The Gothic Cathedral.* Thames & Hudson, London, UK, 1990.